1
Introduction

1.1
Brief Survey of Atmospheric Radiation

The budget of electromagnetic (EM[1)]) radiation in the Earth-atmosphere system is critical to atmospheric energetics. The major portion of energy exchanged between the Earth and the cosmic background, including the solar system, is EM radiation with wavelengths ranging from the ultraviolet (UV) to the far infrared (far IR, FIR) regimes. The transfer of solar and thermal infrared (TIR) radiation, which involves absorption, scattering, and emission in the Earth-atmosphere system, is the primary influence on the terrestrial climate and has a significant impact on the weather system. Atmospheric radiation is an important branch of modern atmospheric sciences because of the role radiation plays in the atmosphere. A number of excellent texts are fully, or partially, dedicated to the discipline of atmospheric radiative transfer including single- and multiple-scattering and absorption processes (Bohren and Clothiaux, 2006; Bohren and Huffman, 1983; Goody and Yung, 1989; Liou, 2002; Mishchenko et al., 2006; Petty, 2006; Pomraning, 1973; Stephens, 1994; Thomas and Stamnes, 1999; Zdunkowski et al., 2007). Some of these texts assume the reader to be well trained in mathematics and physics, particularly in electrodynamics and optics.

The transfer of EM radiation in the atmosphere is a multiple-scattering process involving absorption by various gases along with scattering and absorption by particulate matter (aerosol particles, liquid water droplets, and ice crystals). Early studies of EM radiative transfer were primarily completed by astrophysicists, including the eminent scientists A.S. Eddington, E.A. Milne, K. Schwarzschild, V.A. Ambarzumian, and S. Chandrasekhar, who were interested in the transfer of EM radiation in stellar and planetary atmospheres. Schuster (1905) used a simple two-stream approximation to discuss the transfer of EM radiation through a foggy atmosphere, and is generally believed to be the first to study the multiple-scattering process. However, the study of radiative transfer in a scattering medium can be traced (Mishchenko, 2008) to the work of Lommel (1887) and Chwolson (1889).

1) Acronyms used in this book are written in capital letters and explained in Appendix A.1.

Theory of Atmospheric Radiative Transfer, First Edition. Manfred Wendisch and Ping Yang
© 2012 WILEY-VCH Verlag GmbH & Co. KGaA. Published 2012 by WILEY-VCH Verlag GmbH & Co. KGaA.

The Radiative Transfer Equation (RTE) is the cornerstone of radiative transfer theory. Traditionally, the RTE had been regarded as a phenomenological formula, until the work by Tsang and Kong (2001) and Mishchenko (2008, and references cited therein), who demonstrated the theory of radiative transfer to be a corollary of Maxwell's equations. During the early development stages of the radiative transfer theory, significant effort was dedicated to solving the RTE, subject to the plane-parallel approximation, and the results have been summarized in several classic texts (Chandrasekhar, 1950; Lenoble, 1985; Preisendorfer, 1965; Sobolev, 1975; van de Hulst, 1980).

The RTE for a scattering medium consisting of an ensemble of particles requires an understanding of the interaction between radiation and particulate matter. The Lorenz–Mie theory, first described by Lorenz (1890) with independent subsequent development by Mie (1908) and Debye (1909), was formulated to study the scattering of EM radiation by spherical particles. Logan (1965) surveyed some early, prior to World War II, studies of the scattering of plane EM waves by spheres; however, many atmospheric particles, such as airborne dust aerosol particles and ice crystals, are nonspherical. Within the past fifty years, significant effort (Kokhanovsky, 2006; Mishchenko et al., 2000) has been focused on the description of EM scattering by nonspherical and inhomogeneous particles, resulting in the development of new computational techniques, for example, the T-matrix method (Mishchenko and Travis, 1994b; Waterman, 1965), the finite-difference time domain technique (Yee, 1966), and the discrete dipole approximation (Purcell and Pennypacker, 1973).

The absorption of EM radiation by atmospheric gases has been an active research area with laboratory measurements of various gases documenting spectral line parameters. A long range project, initiated in the 1960s, has compiled and continued updating a High-resolution Transmission Molecular Absorption Database, known as HITRAN (Rothman et al., 1992). Based on HITRAN, the Line-By-Line Radiative Transfer Models (LBLRTMs), for example, see Clough et al. (1992), can accurately compute the transmission of radiation through atmospheric gases, but require substantial computational resources. Various other spectral band models have evolved to increase the computational efficiency of radiative transfer simulation. Other techniques, the *k*-distribution method (Ambartzumian, 1936), the correlated *k*-distribution method (Fu and Liou, 1992b; Lacis and Oinas, 1991; Lacis et al., 1979), the principal component-based radiative transfer technique (Liu et al., 2006), and the optimal spectral sampling method (Moncet et al., 2008), have been developed for both atmospheric radiation budget studies and remote sensing applications.

In the plane-parallel approximation, the optical and microphysical properties of a medium are assumed to be horizontally homogeneous. Attempts to solve the RTE, using the plane-parallel approximation, encountered problems with three-dimensional (3D) radiative transfer, for example, in the transfer of radiation within cumulus clouds. A summary of advances in the study of 3D radiative transfer within cloudy atmospheres can be found in a monograph edited by Marshak and Davis (2005).

Both radiation intensity and polarization properties are required for a complete description of EM radiation. A concise introduction to the transfer of polarized radiation is offered in an excellent treatise by Hovenier et al. (2004). The polarization state of radiation has been employed in the astrophysics and optics disciplines (Mishchenko et al., 2010) for many years; however, atmospheric remote sensing techniques based on polarimetric measurements are in their infancy. The benefits associated with the use of polarization measurements in various passive and active atmospheric remote sensing implementations have become increasingly obvious.

Atmospheric radiation is a rapidly evolving field with new methods and algorithms constantly being developed to solve numerous questions about the radiative transfer process in the atmosphere. The focus of this text will not be on the new developments, but rather on the basic definitions of radiometric and polarimetric quantities and the fundamental principles of atmospheric radiation.

1.2
A Broadbrush Picture of the Atmospheric Radiation Budget

In atmospheric sciences, the EM radiation emitted by the Sun is usually considered to lie within a spectral region of 0.2–5 μm, and is normally referred to as solar radiation; whereas, the terrestrial thermal emission of interest lies within the spectral region primarily from $\sim$ 3 to 100 μm. Both solar radiation and the terrestrial thermal emission have complicated spectral structures, which will be briefly discussed in Section 1.3.

Neglecting the detailed spectral features of the solar spectrum observed at the top of the atmosphere (TOA), Figure 1.1 approximately describes the overall spectral irradiance by the two solid lines calculated by assuming the Sun as a blackbody with a temperature of $T_S = 5800$ K. The two dashed lines in Figure 1.1 represent the terrestrial thermal emission simulated by assuming the effective temperature of the Earth as $T_E = 288$ K without accounting for the absorption of atmospheric gases, such as, carbon dioxide, ozone, and water vapor. The logarithmic scales are applied to the abscissae in Figure 1.1a,b. In Figure 1.1a, the same ordinate scale is applied to both curves; in Figure 1.1b, different scales are applied to the two curves in order to make them appear to be equally manifest. In Figure 1.1b, it is evident that solar radiation is primarily concentrated within a narrow spectral region in comparison with terrestrial thermal emission. The solar and terrestrial spectra are often treated separately in practical applications. As shown in Figure 1.1, the solar spectrum has its maximum within the visible spectral interval of 0.4–0.7 μm and can be perceived by the human eye. The terrestrial thermal emission maximum is located approximately at an infrared (IR) wavelength near 10 μm, which the human eye, without being equipped with a special instrument, cannot see. The locations of the spectral maxima in Figure 1.1 are directly determined by temperature. Stellar radiation has its spectral maximum in the visible region; whereas, the planetary thermal emission has a spectral maximum in the IR region. For this reason, the

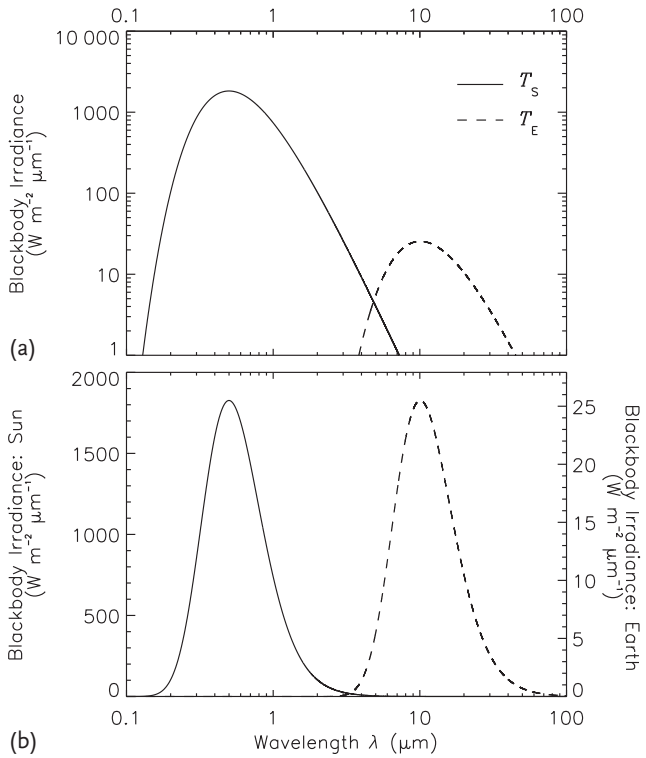

Figure 1.1 (a) Spectra of solar radiation and terrestrial thermal emission simulated by assuming the Sun and the Earth to be blackbodies at temperatures of $T_S = 5800$ K and $T_E = 288$ K. For the spectra, the Planck law, see Eq. (3.58), is applied for isotropic radiation. For the solar spectrum, a mean Sun–Earth distance of 149.6×10^6 km is assumed. (b) The same as in (a), but the left vertical scale is linear and applied to solar spectrum, while the right scale (linear) is applied to the terrestrial thermal emission.

visible color of a star depends on its temperature, and the perceived color of a planet is not determined by its temperature.

Both the solar radiation and the terrestrial thermal emission are modified by several processes before leaving the atmosphere. These processes are illustrated in Figure 1.2 adapted from Trenberth et al. (2009). From the 341 Wm^{-2} of incoming solar radiation, 79 $\mathrm{W\,m}^{-2}$ are reflected back into space by clouds, aerosol particles, and the molecules of atmospheric gases, and 23 $\mathrm{W\,m}^{-2}$ are reflected by the Earth's surface. Thus, a total of 102 $\mathrm{W\,m}^{-2}$, approximately 30% of the solar radiation incident at the TOA, is reflected back into space (left half of Figure 1.2) due to the planetary albedo effect.

Approximately 23%, or 78 $\mathrm{W\,m}^{-2}$, of the solar radiation incident at the TOA is absorbed within the atmosphere. The absorption of solar radiation by atmospheric trace gases, mostly water vapor, contributes to the globally and annually averaged value of 78 $\mathrm{W\,m}^{-2}$. The absorption by aerosol particles and clouds is much less

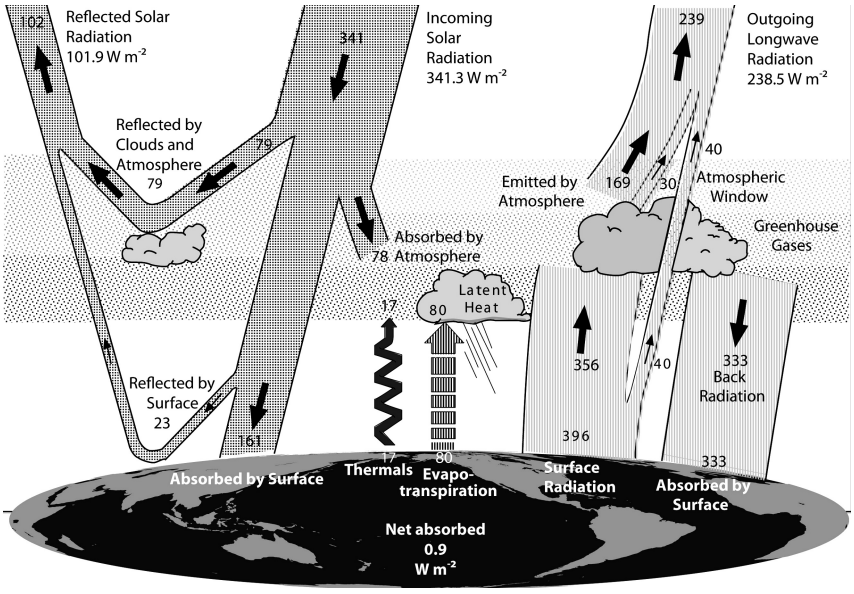

Figure 1.2 The Earth's annual global mean energy budget. The numbers are averaged globally, annually, and wavelength-integrated (broadband-solar: left half of the figure, broadband-thermal: right half) energy flux densities (irradiances) in $\mathrm{W\,m^{-2}}$. Adapted from Trenberth et al. (2009), courtesy of K. Trenberth, and reprinted with permission of the American Meteorological Society (AMS) © AMS.

than that by the gaseous atmospheric components. $161\,\mathrm{W\,m^{-2}}$ ($\approx$ 47%) are absorbed by the land and oceans.

The solar radiation absorbed within the atmosphere and by the surface is transformed into thermal energy (right half of Figure 1.2). Approximately $396\,\mathrm{W\,m^{-2}}$ of the thermal energy is reemitted by the surface, and about $40\,\mathrm{W\,m^{-2}}$ penetrates through the atmosphere in the "atmospheric window regions" without being reabsorbed. Of the surface-emitted terrestrial radiation, about $356\,\mathrm{W\,m^{-2}}$ are absorbed by clouds and trace gases, particularly by water vapor, and reemitted at lower temperatures. Thus, out of the $356\,\mathrm{W\,m^{-2}}$, only $169\,\mathrm{W\,m^{-2}}$ from gases, $30\,\mathrm{W\,m^{-2}}$ from clouds, and $40\,\mathrm{W\,m^{-2}}$ from the surface are reemitted to space. The remaining radiant energy is absorbed by the atmosphere-surface system of the Earth and leads to the greenhouse effect discussed in Section 1.4.

At the TOA, $239\,\mathrm{W\,m^{-2}}$ of terrestrial radiation escapes the Earth-atmosphere system, while the same amount effectively enters the system in the solar spectral region $[(239 = 341 - 102)\,\mathrm{W\,m^{-2}}]$ to maintain the energy equilibrium of the climate system. However, the solar and terrestrial radiation is not in equilibrium at Earth's surface: $(161 - 396 + 333)\,\mathrm{W\,m^{-2}} = 98\,\mathrm{W\,m^{-2}}$. As illustrated in Figure 1.2, the surface continuously gains EM radiant energy, the atmosphere loses radiant energy, and the deficit is balanced by latent and thermal heat transfer.

1.3
Solar and Terrestrial Thermal Infrared Spectra in a Cloudless Atmosphere

Let us take a more detailed look at the downward and upward radiation in a cloud-free atmosphere by observing typical spectra. Figure 1.3 shows the simulated solar spectra observed at both the TOA and the surface. The simulations were performed with the Moderate Spectral Resolution Atmospheric Transmittance Algorithm and Computer Model (MODTRAN), see Berk et al. (1999). The downward solar radiation reveals typical Fraunhofer absorption lines most obvious at the TOA caused by absorption processes in the solar atmosphere. By the time the solar radiation reaches the surface, the EM radiation has been strongly absorbed at selected wavelengths by atmospheric gases, such as the ozone Hartley band (O_3: < 0.31 μm, see Table 8.3), oxygen (O_2: 0.76 μm; O_2-A band), water vapor (H_2O: 0.72, 0.82, 0.94, 1.1, 1.38, 1.87, 2.7 μm, see Table 8.2), or carbon dioxide (CO_2: 1.4, 2.0, 2.7 μm). The pronounced minimum at the 1.38 μm wavelength is caused by water vapor absorption. This water vapor absorption band is very useful for detecting cirrus clouds located high in the atmosphere (Gao and Kaufman, 1995).

Two examples of the spectral distribution of the upward (outgoing) terrestrial IR radiation, corresponding to the surface temperatures 273 and 288 K, at the TOA are presented in Figure 1.4. In some wavelength bands, a cloud-free atmosphere is far from transparent; however, in the 8–13 μm spectral region, the atmosphere is quite transparent except for the ozone absorption band at 9.6 μm. The spectral observations within this atmospheric window region can be used to retrieve typical properties, for example, the surface temperature from space. The strong CO_2 absorption band centered at 15 μm is another distinct feature shown in Figure 1.4.

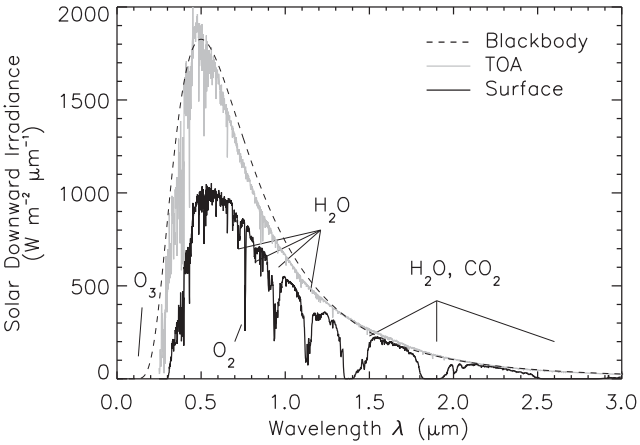

Figure 1.3 Simulated spectral distribution of solar radiation (downward irradiance) at the TOA and at the surface. The dashed line indicates the spectrum by assuming the Sun to be a blackbody with a temperature of $T_S = 5800$ K. The simulations were performed with MODTRAN4 (Version 3 Revision 1, MOD4v3r1) with the Sun in the zenith.

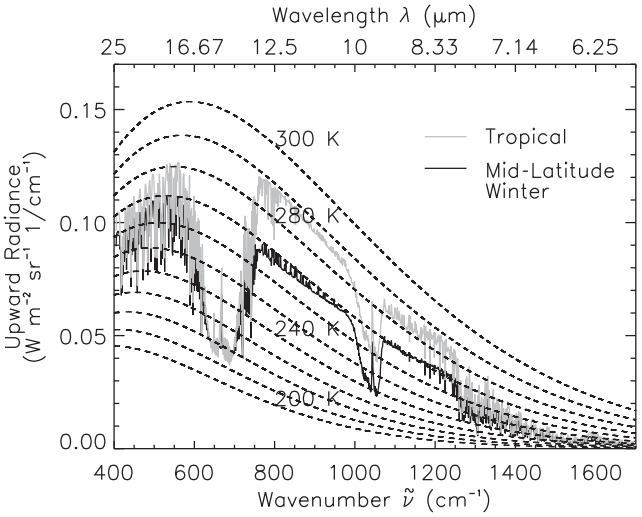

Figure 1.4 Simulated IR upward radiance spectrum at the TOA. "Tropical" and "Mid-Latitude Winter" profiles of atmospheric parameters were applied and taken from Anderson et al. (1986). The dashed lines represent blackbody radiances for various temperatures (200–300 K in 10-K increments). Absorption bands corresponding to CO_2 (15 μm), H_2O (6.3 μm), and O_3 (9.6 μm) are evident. The simulations were performed with MODTRAN4 (Version 3 Revision 1, MOD4v3r1).

Since CO_2 is well mixed and relatively stable in the atmosphere, this absorption band is very useful for the retrieval of the vertical temperature profile.

1.4 The Greenhouse Effect

Spectra of the atmospheric transmissivity along with the downward radiances at the surface are plotted in Figure 1.5. Atmospheric gases (mainly O_2, H_2O, O_3, and CO_2) absorb strongly in certain wavelength regions. However, the atmosphere is quite transparent for a large portion of the solar spectrum, and most of the solar radiation passes through the atmosphere. This is not true for the terrestrial spectral region where much less of the emitted radiation is transmitted through the atmosphere, see Figure 1.6, which shows the spectral signatures of both the transmissivity and the outgoing terrestrial radiance. The spectral signatures result from the variations of the atmospheric gas absorption.

Figure 1.6a,b depict the atmospheric transmissivity in the largest part of the terrestrial wavelength region, and Figure 1.6c,d show the simulated upward emitted radiances at the TOA. In the atmospheric window region between 8 and 13 μm, the atmosphere is essentially transparent to surface emitted radiation. This is more obvious in the comparatively dry (low water vapor amount) vertical profile of the "Subarctic Winter" case (Figure 1.6a) rather than the more humid situation of a "Trop-

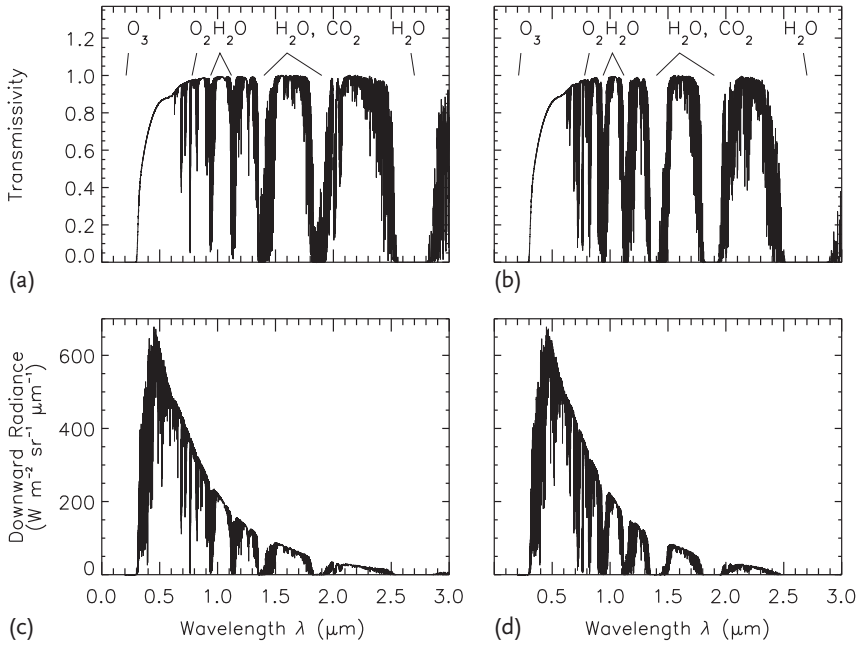

Figure 1.5 Spectral distribution of simulated solar atmospheric transmissivity (a, b) and solar downward radiances at the surface (c, d). "Subarctic Winter" (a, c) and "Tropical" (b, d) profiles of atmospheric parameters were applied and taken from Anderson et al. (1986). Absorption bands corresponding to: O_3: < 0.31 μm; O_2: 0.76 μm; H_2O: 0.72, 0.82, 0.94, 1.1, 1.38, 1.87, 2.7 μm; CO_2: 1.4, 2.0, 2.7 μm, see Table 8.2. The simulations were performed with MODTRAN4 (Version 3 Revision 1, MOD4v3r1) with the Sun in the zenith.

ical" atmosphere (Figure 1.6b). Opposite to the transmissivity, the emitted upward radiances simulated at the TOA (Figure 1.6c,d) are larger for the "Tropical" profile than the "Subarctic Winter" case because the surface temperature is much higher in the "Tropical" case. Outside the atmospheric window region, nearly all terrestrial radiant energy is absorbed by atmospheric trace gases known as greenhouse gases, for example, H_2O, CO_2, and O_3. These gases keep the global temperature approximately 33 K higher than the equilibrium temperature of an atmosphere-free Earth exposed to solar radiation and can be treated as sources of blackbody radiation in certain wavelength regions. Figure 1.6c,d present an illustration of the atmosphere acting as a nonblackbody emitter.

During the last century, the global CO_2 concentration in the atmosphere has been drastically increased by human activities (Keeling et al., 1976), causing a manmade global warming (note, there is an ongoing debate on this subject), the anthropogenic greenhouse effect. In order to stabilize the terrestrial climate system at the preindustrial temperature level, the anthropogenic output of greenhouse gases needs to be significantly decreased.

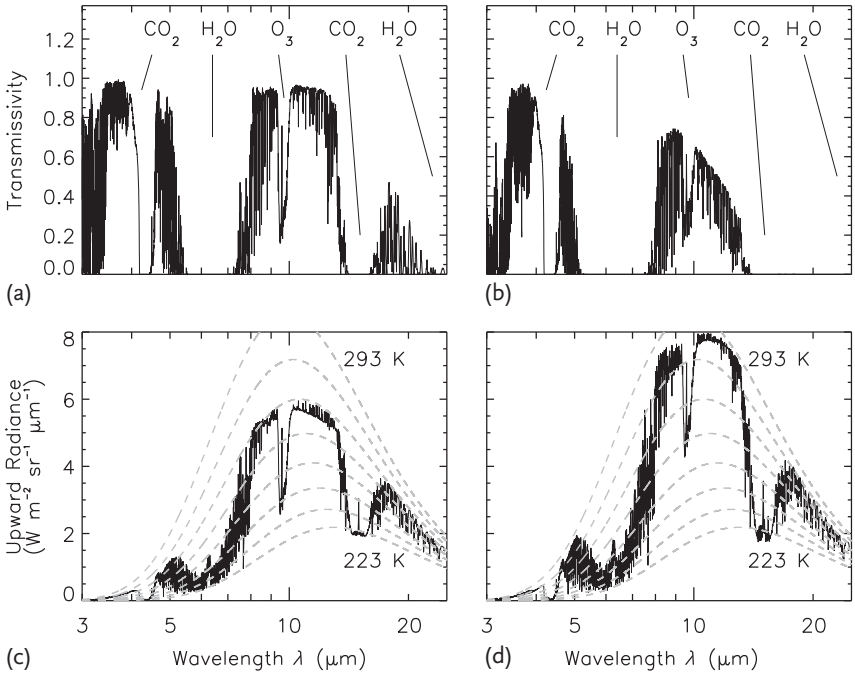

Figure 1.6 Spectral distribution of simulated terrestrial atmospheric transmissivity (a, b) and IR upward radiances emitted at the TOA (c, d). "Subarctic Winter" (a, c) and "Tropical" (b, d) profiles of atmospheric parameters were applied and taken from Anderson et al. (1986). The dashed lines indicate Planck's functions for 293 K (upper curve) and 223 K (lower curve) in 10-K increments. Major absorption/emission bands corresponding to: CO_2: 4.3, 15 μm; H_2O: 6.3 μm; O_3: 9.6 μm. The simulations were performed with MODTRAN4 (Version 3 Revision 1, MOD4v3r1).

1.5 Relevance to the Interpretation of Spaceborne Observations

Global scale observations of the Earth's atmosphere, oceans, and land surfaces are needed to study the planet as an unseparated system. Satellite observations provide unprecedented data sets to study numerous dynamic, physical, and chemical processes in the Earth-atmosphere system. The satellite instruments are designed to detect EM radiation in various spectral regions. The EM radiation signals received by satellite sensors need interpretation to decipher the processes that govern the transfer of EM radiation through the atmosphere and to separate the influences of ocean and land surfaces.

Two major types of spaceborne instruments, passive receivers and active sensors, are deployed on orbiting satellites. Passive receivers detect radiation reflected or emitted by atmospheric constituents, such as, gas molecules, aerosol particles, and cloud or precipitation elements. The signals recorded by the passive satellite receivers can be used to retrieve atmospheric parameters, such as, temperature

profiles, wind and humidity fields, aerosol properties, and cloud characteristics. Additionally, they are able to measure the components of the solar and terrestrial radiation budget. The active instruments, for example, LIDAR and RADAR, emit EM radiation and measure the backscatter from the initial radiation beams, which contains atmospheric property information. Examples of advanced spaceborne sensors are those on the "A-train" satellite platforms (Stephens et al., 2002).

To properly interpret spaceborne observations made by either passive or active instruments, knowledge of atmospheric radiative transfer and of the interactions between radiation and atmospheric constituents of interest is required. The basic principles of atmospheric radiation will be covered in this text to help one understand the fundamental principles of spaceborne atmospheric remote sensing.